# CHAPTER 5

# JANUARY AND JULY CLIMATE SIMULATIONS OVER SOUTHERN AFRICA USING DARLAM

## 5.1 INTRODUCTION

Chapter 5 describes the results of climatological simulations over the SADC region with DARLAM. The LAM is one-way nested within simulations of selected months (January and July) from a long seasonal varying simulation of the CSIRO9 AGCM (both models are discussed in Chapter 3). The relatively coarse resolution (spectral resolution of R21) AGCM with 9 levels in the vertical is used to provide boundary conditions to DARLAM, which is run at a horizontal grid resolution of 60 km with 18 levels in the vertical. The AGCM supplies large-scale synoptic forcing to DARLAM through its lateral boundaries. DARLAM's dynamical formulation and physical parameterisation schemes are similar to those used in the AGCM but it's higher resolution adds significant smaller-scale detail to the coarser simulation of the AGCM. This chapter will illustrate that the additional detail provides improved simulation results, when compared to AGCM results over most regions of the LAM domain.

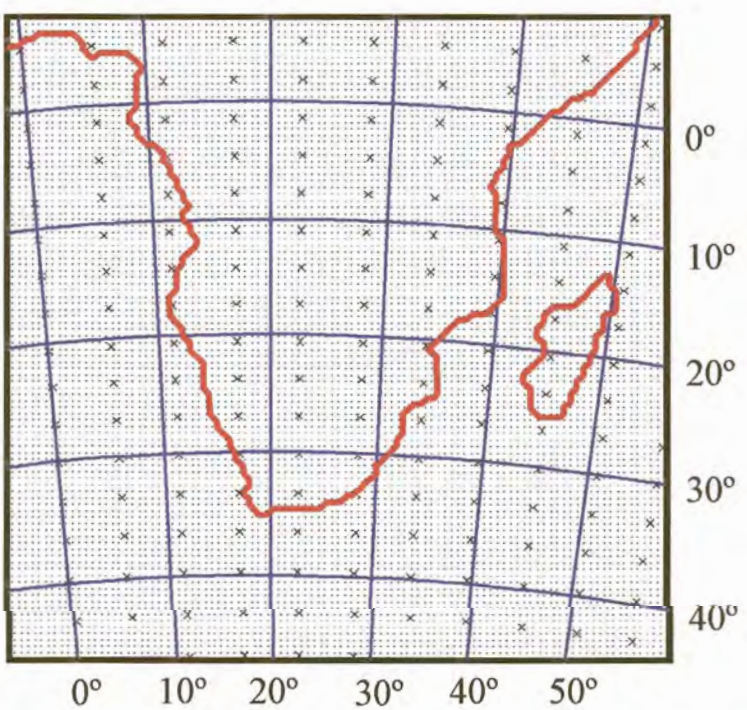


**Figure 5.1** DARLAM domain used for the simulations over the SADC region. The 60 km x 60 km spaced nested model grid points (on a Lambert conformal projection) are indicated by dots. Gaussian grid points of the R21 CSIRO9 AGCM are indicated by crosses.

The DARLAM domain covers the entire SADC region. Therefore, an important feature of the simulations is the inclusion of extensive regions north and south of the equator (see section 2.3.1). It might be expected that DARLAM would perform better over mid-latitude than tropical regions. Weather systems generally move slower in tropical regions and internal quasi-stationary systems may evolve within the nested model domain independent of the boundary forcing (Walsh and McGregor, 1995, also see section 2.3.1). It is also worthwhile to note that large regions of southern Africa are influenced by both tropical and mid-latitude systems. The LAM's domain size (figure 5.1) is considerably larger and both the horizontal and vertical resolution much finer than used in any previously performed climate simulations over the SADC region. The results presented here also include the first July climate simulations over the SADC region.

The DARLAM simulations of climate for January (the peak rainfall month over southern Africa) and July are qualitatively compared with observations as well as results from the AGCM. Of interest is the extent to which boundary forcing supplied by the AGCM influences nested model simulations, as well as the extent to which the higher resolution of the nested model results in improved climate simulations of surface and lower-tropospheric conditions over the region.

## 5.2 EXPERIMENTAL DESIGN AND VALIDATION DATA

A one-way nesting technique is used in these experiments. Every 12 hours lateral boundary conditions are supplied by the CSIRO9 AGCM. At each time step the outermost DARLAM boundary grid rows are relaxed toward interpolated AGCM values. The nesting procedure of Davies (1976) is used, but with exponentially decreasing weights. Initial atmospheric conditions for DARLAM (including soil moistures) are supplied by the forcing AGCM and SSTs are prescribed every 12 hours by the AGCM.

Nine separate 30-day simulations have been performed for both January (mid-summer) and July (mid-winter). The averages of these simulations constitute the model climatology for these months. The 30-day simulations incorporated both diurnal and seasonally varying radiation but were initialised separately with output fields taken from the CSIRO9 AGCM. No vertical-mode initialisation has been performed. A short spin-up period of about two days allowed for the moisture cycle to reach equilibrium. Similar experiments over the Australian region indicated that the spin-up process has a negligible effect on the DARLAM climate (Walsh and McGregor, 1995). For surface pressure and temperature the boundary fields are altered to compensate for any differences in height that may arise in the interpolated topography of the AGCM relative to DARLAM.

In this study January resembles mid-summer (austral summer) conditions, since it has been shown that most of southern Africa receives a pronounced summer rainfall maximum during January (Tyson, 1986). July represents mid-winter conditions. Mean circulation, temperature and rainfall fields as

simulated by both the AGCM and LAM are compared to observed fields. Observed mean sea-level pressure (MSLP), 10 m u and v wind components, 2m-temperature and rainfall were obtained from 4-hourly NCEP (National Centre for Environmental Prediction) reanalysis data (Kalnay et al., 1996). The fields constitute 40-year (1958-1998) mean monthly climatologies for January and July on a 2.5°x 2.5° grid resolution. The relatively low spatial resolution of the observed data compared to the 60 km resolution of DARLAM renders the data unsuitable for quantitative model verification.

DARLAM simulations has been performed on a Pentium III computer with two 550 MHz processors. It took 11-minutes (CPU time) to simulate a model day at 60 km resolution with 18 levels in the vertical. An advective time step of 15 minutes was used.

## 5.3 MODEL TOPOGRAPHY

The interior of South Africa is characterised by an elevated plateau with altitudes in excess of 1000 m. Maximum altitudes in excess of 3500 m occur along the South African eastern escarpment, as well as over Tropical East Africa. The coastal margins along the east and south-east coast of southern Africa are narrow and marked by steep topographic gradients. The R21 spectral resolution of the CSIRO9 AGCM uses a significantly smoothed topography as lower altitude boundary (figure 5.2a). The plateau is narrow and maximum altitudes are under-estimated by as much as 2500 m. Topographic gradients along the escarpment are also very gentle (figure 5.2a). In the AGCM's representation the topography of Madagascar is poorly resolved and extremely smooth over the entire island. Islands such as Mauritius and La Reunion are not even captured by the AGCM topography. The spectral method requires that the surface topography is spectrally fitted to a wave resolution of R21. The initial observed topography consists of a 1°x1° data set that is spatially averaged to the 64x56 global Gaussian grid of the CSIRO9 AGCM, and then spectrally resynthesized to R21 resolution (McGregor et al., 1993a). A consequence of this procedure is non-zero and even negative sea elevation (blue regions in figure 5.2a) which is caused by the Gibbs phenomenon (McGregor et al., 1993a).

With a horizontal resolution of 60 km, DARLAM provides a more detailed representation of observed regional topographic features over southern Africa (figure 5.2b). More realistic maximum elevations occur over the escarpment of south-eastern South Africa (in excess of 2400 m above sea level) and Tropical East Africa (in excess of 3000 m above sea level). In general, DARLAM contains much more detail at 60 km resolution than found in the associated AGCM topography field, for example features such as steep topographic gradients along the southern African escarpment and the Namibian highlands are well captured. The eastern mountain ranges of Madagascar are more obvious and realistic. Even smaller islands such as Mauritius, La Reunion and the Comoros are visible in the DARLAM topography field (not shown). This is a significant improvement on the AGCM topography.

Experiments performed over Australia (McGregor and Walsh, 1993) indicated that climate simulations by LAMs are significantly improved by a better representation of topography (also see Chapter 3).

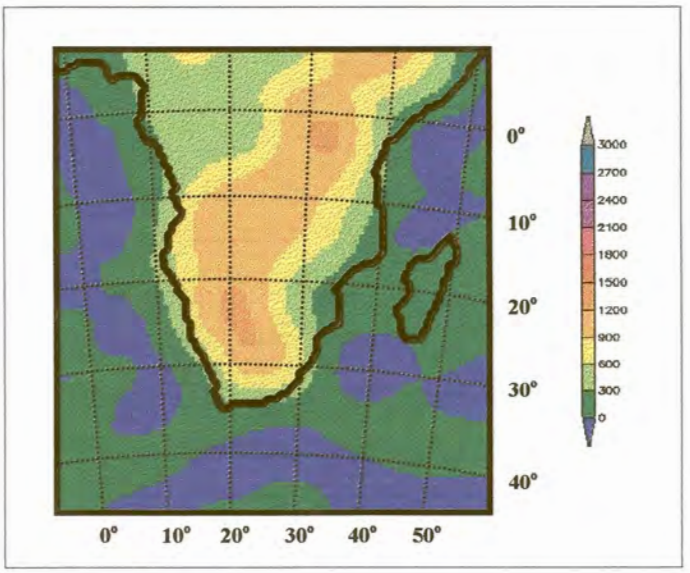


**Figure 5.2a** CSIRO AGCM representation of topography at R21 spectral resolution over the SADC region. The contour interval is 300 m. Note the smoothed elevation over land and negative elevation over the oceans.

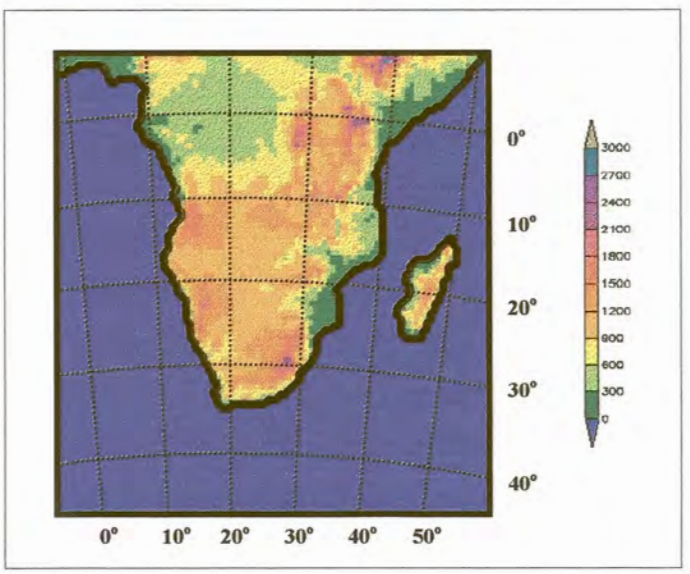


**Figure 5.2b** DARLAM representation of topography at a 60 km grid point resolution over the SADC region. The contour interval is 300 m. The additional detail is a significant improvement over the AGCM topography.

## 5.4 MODEL OUTPUT RESULTS

### 5.4.1 MEAN SEA-LEVEL PRESSURE

Characteristic features of the observed mean sea-level pressure (MSLP) distribution over the SADC region and adjacent oceans are illustrated in figures 5.3a (January) and 5.3b (July).

The January MSLP distribution over the SADC region is characterised by a deep continental low-pressure system (heat low) located at 25°S over Botswana and Namibia and two well-defined anticyclones over the oceans adjacent to the subcontinent (figure 5.3a). A well-developed meridional pressure gradient is present to the south of South Africa where the pressure drops toward the circumpolar trough. Lower pressures occur over the tropical subcontinent during January (figure 5.3a), which indicate the location of the southern extension of the Intertropical Convergence Zone (ITCZ). The relative higher MSLP recorded over south-eastern South Africa and eastern Madagascar during January (figure 5.3a) are the result of migrating high-pressure systems that frequently ridge to the south of the African continent during summer seasons.

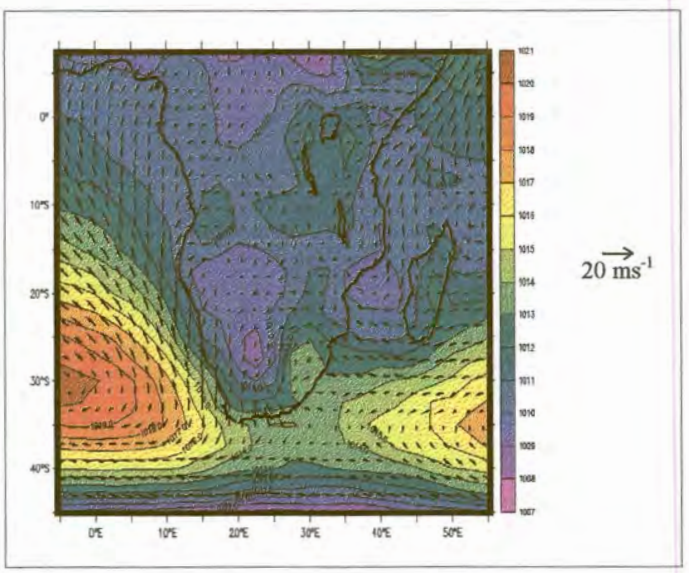


**Figure 5.3a** Observed mean sea-level pressure (MSLP) measured in hPa and wind vectors (at 10 m altitude) meassured in $ms^{-1}$ for January as obtained from a 40-year (1958 to 1998) NCEP reanalysis climatology. The pressure contour interval is 1 hPa.

During the austral winter (July) the observed oceanic anticyclones intensify and shift northward. At the same time a well-developed high-pressure belt develops over the subcontinent (figure 5.3b). The meridional pressure gradient to the south of South Africa increases as a result of the deeper circumpolar trough, causing westerly winds to intensify over this region. Over

tropical regions south of the equator pressures are generally higher in association with the northward propagation of the ITCZ during winter.

The semi-stationary low-pressure cell (a trough in July) present in the NCEP reanalysis field over the Mozambique channel (figures 5.3a and 5.3b) can be regarded as a giant lee low that originates downwind of the eastern Madagascar mountain range in the persistent easterly wind flow (wind vectors in figure 5.3a and 5.3b). The amplitude of this trough and its southward extent decrease in the austral winter (fig 5.3b). The increased amplitude and greater southward extent during January is likely to result from the observed southward shift of the south-easterly trade wind regime during the austral summer, in association with the usual simultaneous occurrence of relative higher SSTs in the Mozambique channel.

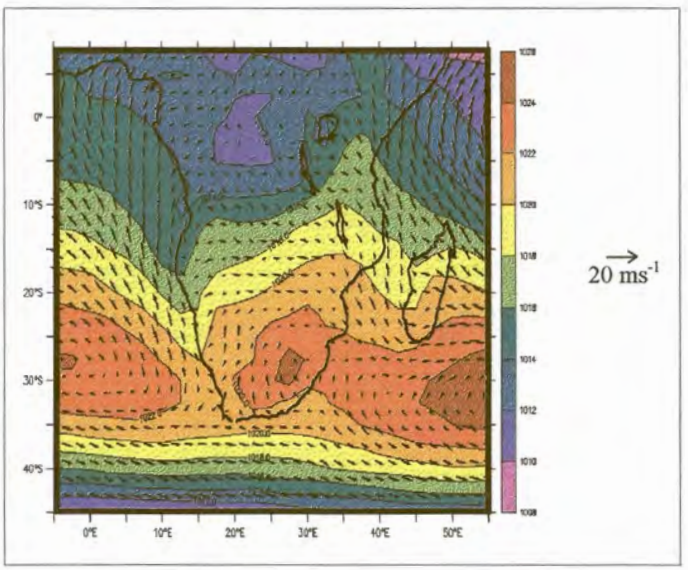


**Figure 5.3b** Observed mean sea-level pressure (MSLP) measured in hPa and wind vectors (at 10 m altitude) measured in $ms^{-1}$ for July as obtained from a forty year (1958 to 1998) NCEP reanalysis climatology. The pressure contour interval is 2 hPa.

The general synoptic-scale features of the observed MSLP are adequately captured in the CSIRO9 AGCM simulations for January and July (figures 5.3c and 5.3d).

In the January simulation (figure 5.3c), the low-pressure cell over Namibia and Botswana is located further to the north and west than observed, although the intensity of the cell is well reproduced. The relative position (also meridional position) of the oceanic anticyclones is well captured. The amplitudes of both these cells however, are overestimated. The meridional pressure gradient to the south of South Africa, as simulated by the CSIRO9 AGCM, closely corresponds to the observed gradient. The CSIRO9 AGCM overestimates MSLPs over tropical regions and fails to reproduce the presence of lower

pressures in the Mozambique Channel. MSLPs over the Mozambique Channel are severely overestimated (by as much as 4 hPa). The CSIRO9 AGCM also fails to capture the pattern of relatively higher MSLPs over the south-eastern part of South Africa and eastern Madagascar.

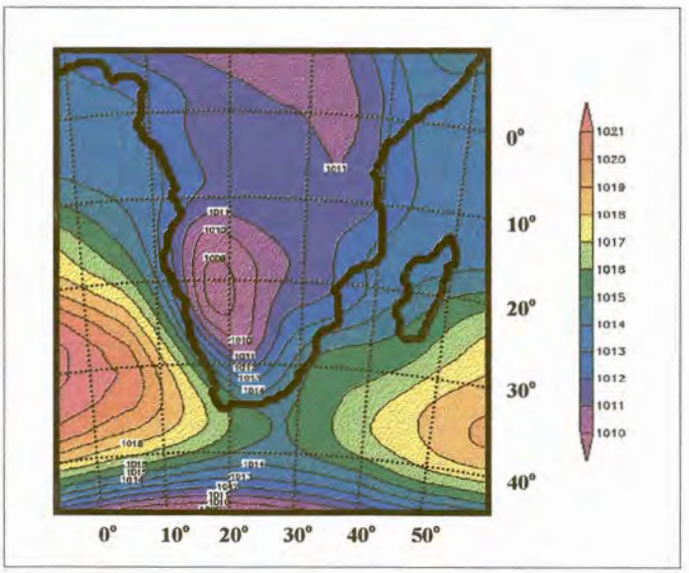


**Figure 5.3c** Mean sea-level pressure (MSLP) measured in hPa for January as simulated by the CSIRO9 AGCM. The pressure contour interval is 1 hPa.

The CSIRO9 AGCM successfully simulates the observed northward shift and intensification of the subtropical anticyclones in July, as well as the tighter meridional pressure gradient associated with the deeper circumpolar trough (figure 5.3d). The simulation of amplitudes of the broader July MSLP pattern is weaker when compared to the simulation of January amplitudes. In particular, the intensity of the Indian Ocean high-pressure system is underestimated by more than 4hPa. As found in the January simulations, the CSIRO9 AGCM simulates higher than observed MSLPs over the tropical regions and again fails to simulate the trough in the Mozambique Channel. The July CSIRO9 AGCM simulation however, does capture the higher pressures over tropical regions south of the equator (relative to January) suggesting that the model succeeds in simulating the northward displacement of the ITCZ during the austral winter.

DARLAM is forced at the lateral edges of its domain by boundary conditions supplied by the CSIRO9 AGCM. The January and July MSLP patterns as simulated by the LAM (Figure 5.3e and 5.3f) are therefore similar to those of the CSIRO9 AGCM. As a matter of fact the two model simulations have much in common, especially over maritime regions where the higher resolution surface topography of the LAM is absent. The lower intensities of the two subtropical oceanic high-pressure systems, as simulated by DARLAM for

January, are slightly more accurate than in the corresponding CSIRO9 AGCM simulations (compare figures 5.3a, 5.3c and 5.3e).

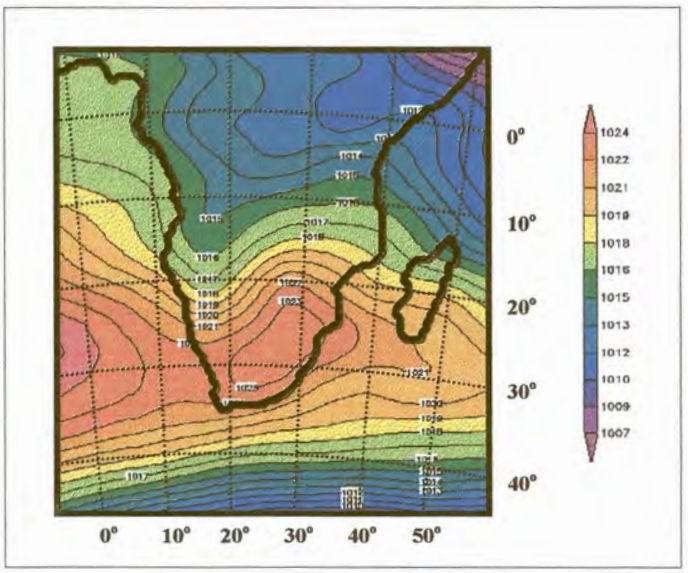


**Figure 5.3d** Mean sea-level pressure (MSLP) measured in hPa for July as simulated by the CSIRO9 AGCM. The pressure contour interval is 1 hPa.

The DARLAM continental low over the western subcontinent is larger in extent and slightly deeper than found in CSIRO9 AGCM simulations. The low simulated by DARLAM also extends further to the south and east. The centre of the low (figure 5.3e) is in close correspondence with the observed position (figure 5.3a), which represents a significant improvement over the AGCM simulation (figure 5.3c).

The DARLAM simulations of MSLP over southern Africa and Madagascar contain far more detail than the corresponding CSIRO9 AGCM simulations. DARLAM adequately simulates the observed pattern of high-pressure intrusion over the south-eastern parts of South Africa and Madagascar (compare figures 5.3a and 5.3e). This may be explained by the fact that the high resolution topography in DARLAM enables the model to capture low-level mass convergence along the south-eastern escarpment of South Africa and Madagascar when high pressure systems ridge to the south of Africa. The AGCM, with its smooth topography, is unable to capture this pattern (compare figures 5.3c and 5.3a).

Another outstanding feature in the DARLAM simulation is the reproduction of the observed low in the Mozambique Channel. Altitudes in the DARLAM topography over Madagascar are in excess of 1200 m (figure 5.2b), which is sufficient to capture the development of a gigantic lee low that is located downwind of the Madagascar mountain range. DARLAM underestimates the intensity of the low, however. This low does not exist in the CSIRO9 AGCM simulation probably as a result of the smoothed topography (figure 5.2a).

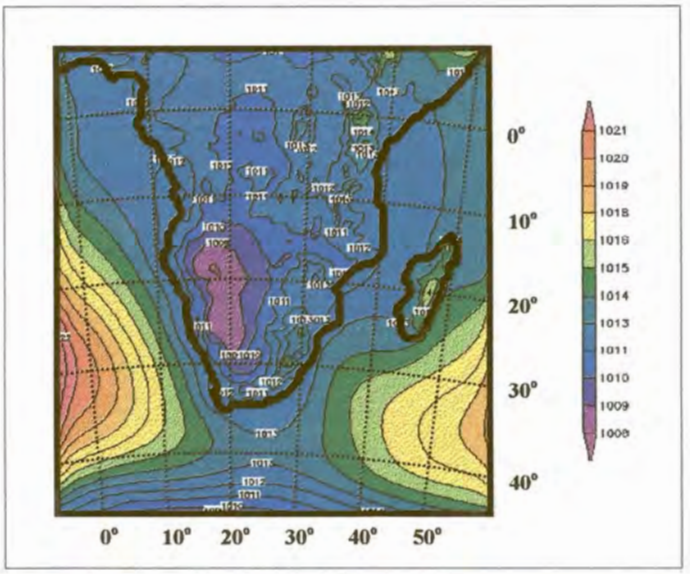


**Figure 5.3e** Mean sea-level pressure (MSLP) measured in hPa for January as simulated by DARLAM. The pressure contour interval is 1 hPa.

July MSLP simulations by DARLAM (figure 5.3f) indicate an underestimation of the intensity of the Indian Ocean high-pressure system similar to that of the forcing AGCM. Over tropical regions DARLAM generally simulates lower MSLPs (that are in close correspondence with the observed pattern) than the AGCM. DARLAM severely underestimates the intensity of the subtropical high-pressure belt over the African continent (by as much as 6 hPa), as well as the intensity of the meridional pressure gradient to the south of Africa. In this respect DARLAM simulations are inferior to the associated CSIRO9 AGCM simulations.

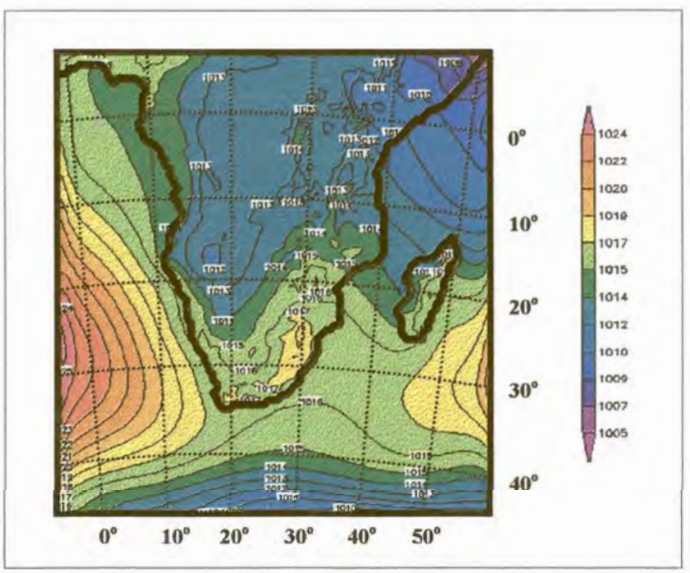


**Figure 5.3f** Mean sea-level pressure (MSLP) measured in hPa for July as simulated by DARLAM. The pressure contour interval is 1 hPa.

### 5.4.2 LOW-LEVEL WIND PATTERNS

The climatology of wind vectors from the NCEP reanalyses data at an altitude of 10 m is superimposed upon the MSLPs in figures 5.3a (January) and 5.3b (July). This is regarded as observed patterns. The associated model simulated streamlines on the lowest model levels ($\sigma = 0.98$) are illustrated in figures 5.4a and 5.4b (for the CSIRO9 AGCM) and 5.4c and 5.4d (for DARLAM).

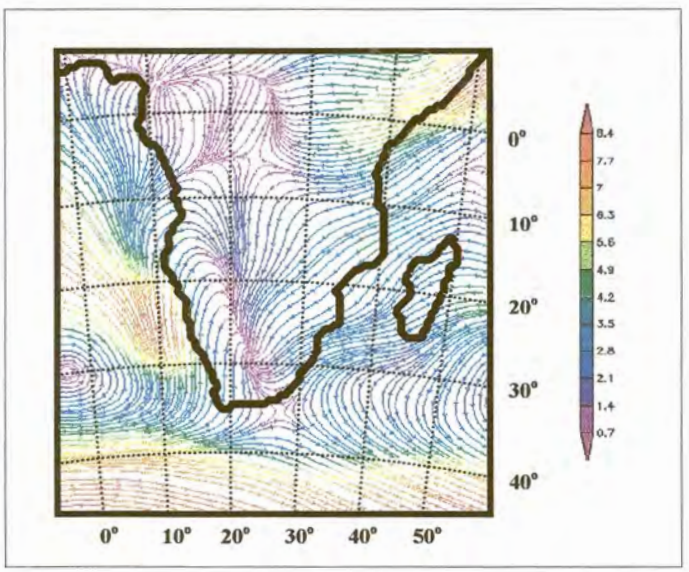


**Figure 5.4a** Mean streamlines at the lowest model level ($\sigma = 0.98$) measured in $m.s^{-1}$ for January as simulated by the CSIRO9 AGCM.

The CSIRO9 AGCM does not capture the observed low-level convergence in the Mozambique Channel that usually occurs during January in association with the low over the area (compare figures 5.3a and 5.4a). This flow deficiency may be attributed to the inadequate, smooth topography of Madagascar used in AGCM simulations (figure 5.2a). With a more detailed topography, it is anticipated that DARLAM will provide improved streamline simulations.

Both DARLAM and the CSIRO9 AGCM reproduce the zone of convergence over the western parts of southern Africa (figures 5.4a and 5.4c). The convergence is associated with the observed continental low that usually develops over Namibia and Botswana during the austral summer. However, over the central and eastern interior of South Africa, the CSIRO9 AGCM produces north-easterly flow (figure 5.4a) whilst DARLAM simulates a pronounced northerly flow (figure 5.4c). The NCEP reanalysis, or observed winds (figure 5.3a), are in favour of the DARLAM simulation of a dominant northerly component in the flow to the west of the eastern escarpment of South Africa. The northerly flow probably results from an interaction between the counter-clockwise circulation around the Indian high and continental low-pressure systems (continental troughs). In addition, DARLAM also successfully simulates the observed higher pressures over the eastern

escarpment of South Africa (section 5.4.1), a feature that does not occur in the CSIRO9 AGCM simulation. In this respect it is also worthwhile noting that in reality the topography of Madagascar turns north-easterly flow, which prevails over the ocean to the east of the island, into easterly flow over the Mozambique Channel (figure 5.3a). DARLAM captures this phenomenon (figure 5.4c) but the CSIRO9 AGCM, with its smooth topography, persists with north-easterly flow over the Mozambique Channel and eventually also over the eastern parts of South Africa (figure 5.4a). In fact, south of 20°S over the coast of Mozambique, south-easterly flow can be observed (figure 5.3a). DARLAM simulates easterly flow over this area (figure 5.4c) but the AGCM persists with north-easterly streamlines (figure 5.4a).

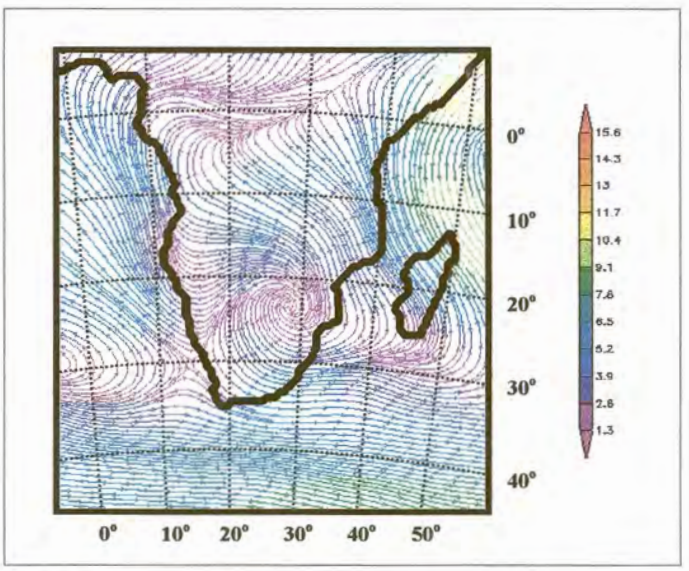


**Figure 5.4b** Mean streamlines at the lowest model level ($\sigma = 0.98$) measured in $m.s^{-1}$ for July as simulated by the CSIRO9 AGCM.

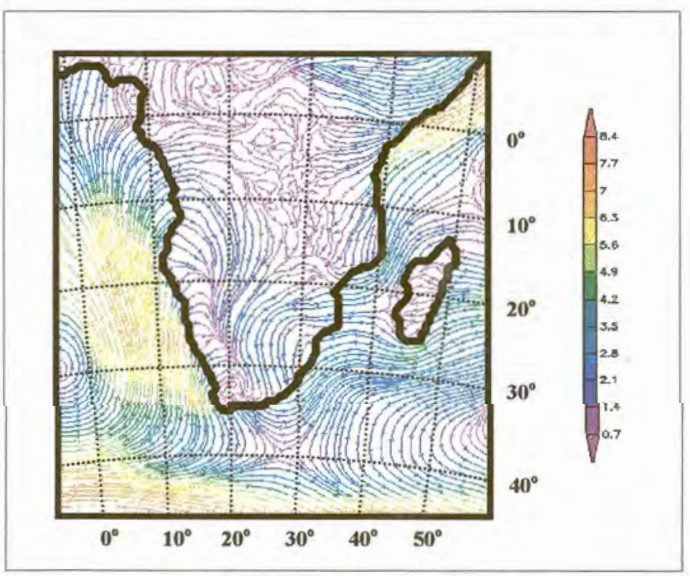


**Figure 5.4c** Mean streamlines at the lowest model level ($\sigma = 0.98$) measured in $m.s^{-1}$ for January as simulated by DARLAM.

Compared to the CSIRO9 AGCM, DARLAM simulates weaker low-level westerly flow to the south of Africa in both the January and July climatologies (figures 5.4a, 5.4b, 5.4c and 5.4d). The observed flow is in general stronger than simulated by both DARLAM and the CSIRO9 AGCM. The weaker DARLAM flow is more obvious in the July simulation when DARLAM also underestimates the meridional pressure gradient to the south of South Africa, as well as the intensity of the subtropical high pressure belt over the interior of South Africa (figure 5.3f).

For July both the models reproduce the observed winter offshore flow over the eastern parts of South Africa (figures 5.3b, 5.4b and 5.4d). The offshore flow is a result of counter-clockwise rotation in the subtropical high-pressure zonal belt over the region (figure 5.3b, 5.3d and 5.3f). Once again DARLAM improves on the AGCM simulation by capturing the cyclonic flow around the trough that is situated over the western parts of Madagascar (figure 5.3b and 5.4d).

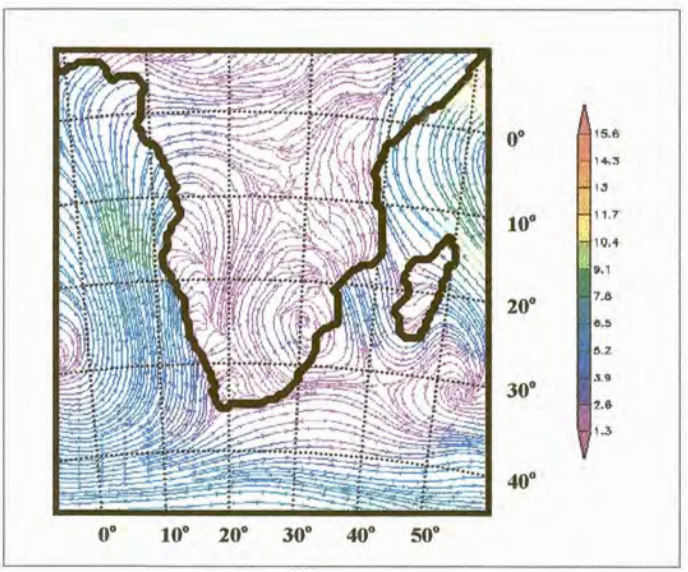


**Figure 5.4d** Mean streamlines at the lowest model level ($\sigma = 0.98$) measured in $m.s^{-1}$ for July as simulated by DARLAM.

### 5.4.3 SURFACE TEMPERATURE

Figure 5.5a and 5.5b provide some detail concerning the observed features of near surface air temperature distribution over the SADC region and adjacent oceans. During January and July a well-defined meridional temperature gradient is present over the region. The gradient is obviously stronger during the austral winter (figure 5.5b). Temperatures are lower over the Atlantic Ocean (where the cold Benguela ocean current is associated with upwelling along the western coastline of southern Africa) than over the Indian Ocean. In the Mozambique Channel, where the warm Agulhus ocean current flows southward, warmer temperatures likewise intrude far to the south.

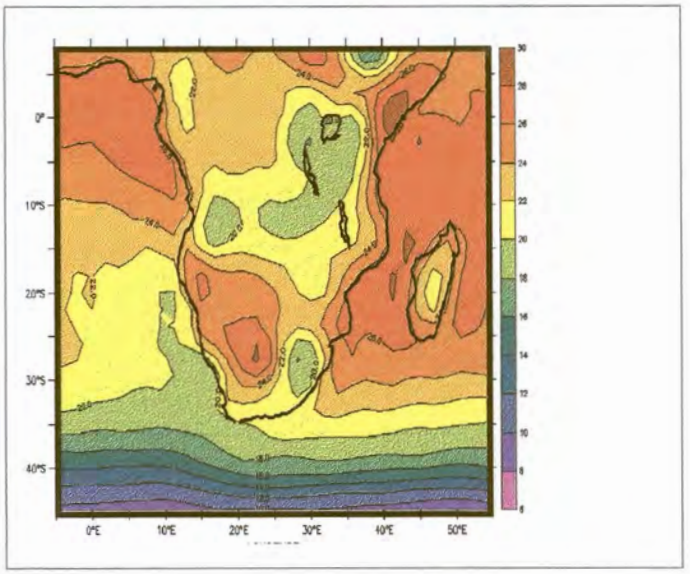


**Figure 5.5a** Observed 2m-temperature climate measured in °C for January as obtained from a 40-year (1958 to 1998) NCEP reanalysis climatology. The temperature contour interval is 2 °C.

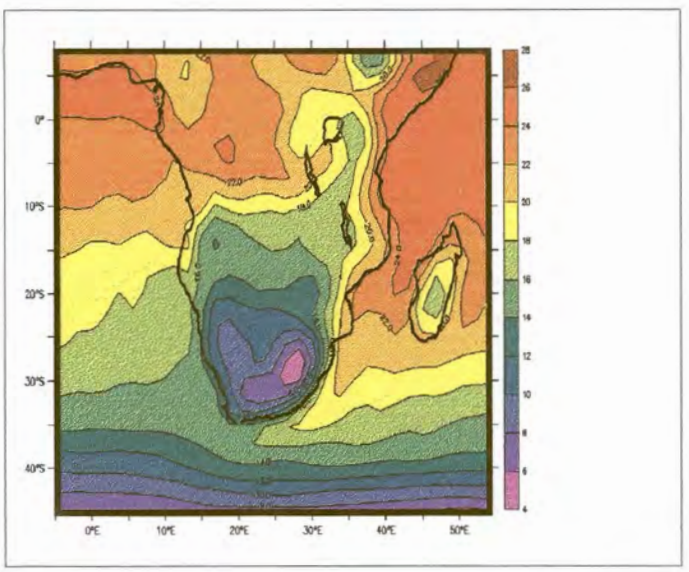


**Figure 5.5b** Observed 2m-temperature climate measured in °C for July as obtained from a 40-year (1958 to 1998) NCEP reanalysis climatology. The temperature contour interval is 2 °C.

During January temperature maximums in excess of 28°C are observed in Tropical East Africa, the western interior of South Africa, Botswana and in the Mozambique Channel (figure 5.5a). In both the January and July fields the influence of topography on near surface temperature over the south-eastern interior of South Africa is well illustrated. Colder isoterms from the south extend northward over this high altitude region. The steep escarpment along

the south-eastern part of South Africa is also associated with steep temperature gradients, especially during the austral winter (figure 5.5b) when maximum insolation shifts northwards and topographic effects become more profound. The eastern Madagascar mountain range has a similar effect on temperature distribution over the island (figures 5.5a and 5.5b).

When comparing CSIRO9 AGCM and DARLAM simulated temperatures it is important to keep in mind that the AGCM simulations represent surface temperatures, whilst DARLAM and NCEP data are screen height (2m) air temperatures. This explains why the CSIRO9 AGCM temperatures are, on average, a degree or two higher than those of the other two fields. In general, simulations from the two models have specific similarities but there are also some major differences. DARLAM contains a more detailed representation of the land/ocean boundary. This is especially noticeable along the western coastline, where the change in near surface temperature is more abrupt in the LAM simulations (figures 5.5e and 5.5f) compared to those of the CSIRO9 AGCM (figures 5.5c and 5.5d). Both models capture the observed meridional temperature gradient, the northward intruding temperatures along the western coastline, as well as the southward extending warmer temperatures along the eastern coastline.

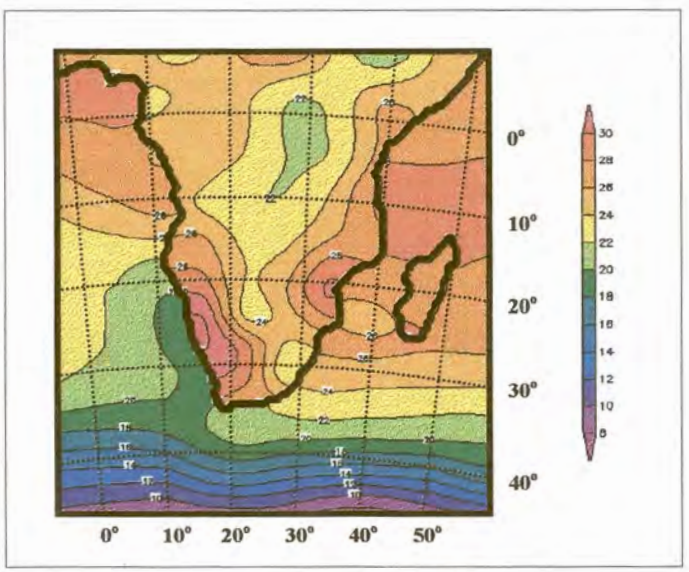


**Figure 5.5c** Surface temperature climate measured in °C for January as simulated by the CSIRO9 AGCM. The temperature contour interval is 2 °C.

Compared to the CSIRO9 AGCM simulations, DARLAM temperature patterns are in general closer to the associated observed patterns over the landmasses. DARLAM reproduces the observed January temperature maximums over the western interior of South Africa, Botswana, Tropical East Africa and the northern part of the Mozambique Channel (figure 5.5e). Note that DARLAM underestimates these temperature maximums by a degree or two. The CSIRO9 AGCM, however, spuriously simulates temperature maximums for January (figure 5.5c) in a broad band over Namibia at the lee

side of the smoothed AGCM model plateau (figure 5.2a). The AGCM also fails to simulate the temperature maximum observed over Tropical East Africa during January. This might be attributed to the fact the low-altitude Great Eastern African Valley topography with the associated higher maximum temperatures is not embedded in the smoothed AGCM topography (figure 5.2a). The higher resolution DARLAM topography does resolve this feature (figure 5.2b) resulting in a significantly improved simulation of near surface temperature over the region (compare figures 5.5c and 5.5e to 5.5a). Both DARLAM and the CSIRO9 AGCM underestimate temperatures over the Mozambique Channel in January.

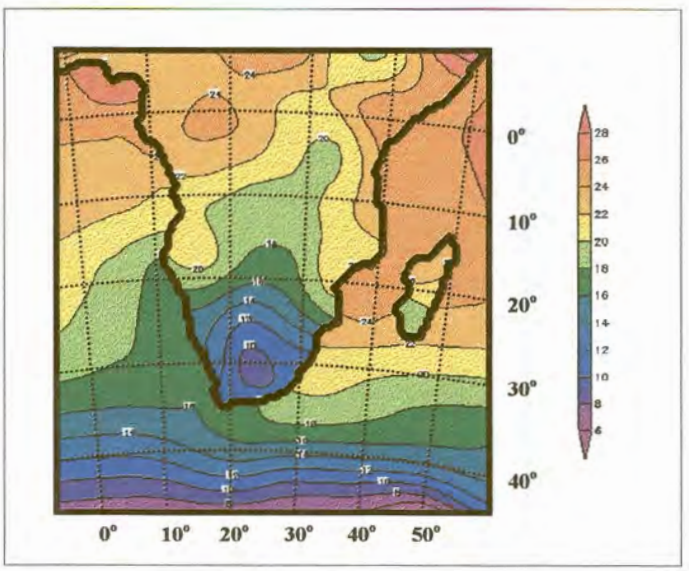


**Figure 5.5d** Surface temperature climate measured in °C for July as simulated by the CSIRO9 AGCM. The temperature contour interval is 2 °C.

Both models capture the observed intrusion of colder isoterms over the south-eastern interior of South Africa that usually occur during January and July. Over this region DARLAM July temperature simulations (figure 5.5f) compare well with observations (figure 5.5b). DARLAM however, severely overestimates the occurrence of colder temperatures over the south-eastern interior of South Africa in January. Analysis of DARLAM rainfall simulations (discussed in the next section) indicates that DARLAM severely overestimates rainfall totals over this region. The overestimation of rainfall may be responsible for the underestimation of screen temperature as a result of severe evaporative cooling at the model surface.

In both the January and July simulations DARLAM successfully captures the observed west-east temperature gradient over Madagascar (figures 5.5e and 5.5f), a feature that does not occur in the corresponding AGCM simulations (figures 5.5c and 5.5d). DARLAM simulates lower than observed temperatures over eastern Madagascar. As an air mass in the dominant easterly flow over Madagascar descends on the lee side of the mountain

range, it will warm adiabatically to produce higher near surface temperatures over the western parts of Madagascar. It seems as if the adiabatic heating (bergwinds) is adequately reproduced in DARLAM simulations, while the CSIRO9 AGCM with its smoothed topography reduces the influence of surface elevation on the general circulation and temperature distribution.

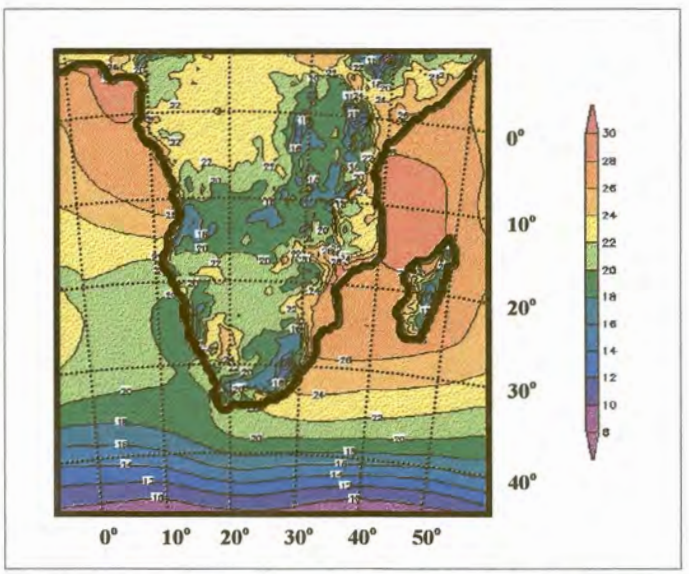


**Figure 5.5e** 2m-temperature climate measured in °C for January as simulated by DARLAM. The temperature contour interval is 2 °C.

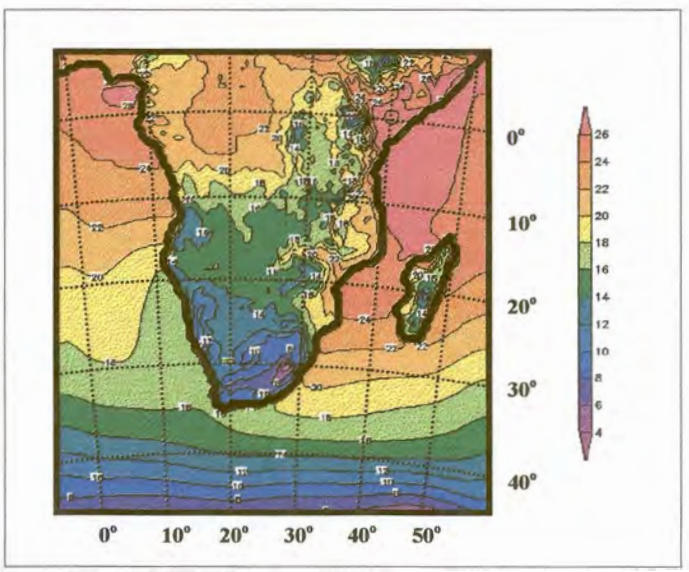


**Figure 5.5f** 2m-temperature climate measured in °C for July as simulated by DARLAM. The temperature contour interval is 2 °C.

### 5.4.4 RAINFALL

The climatology of rainfall from the NCEP reanalyses data provide some indication of the observed rainfall distribution over the SADC region during January (figure 5.6a) and July (figure 5.6b).

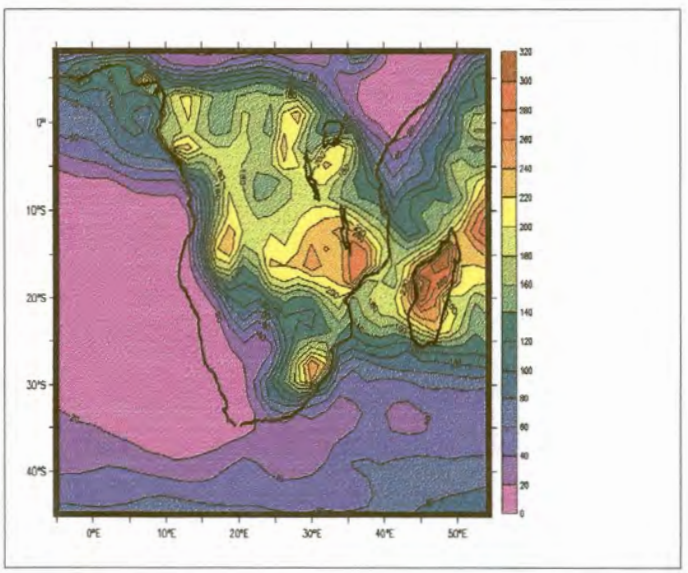


**Figure 5.6a** Observed rainfall total climate measured in mm for January as obtained from a 40-year (1958 to 1998) NCEP reanalysis climatology. The rainfall contour interval is 20 mm.

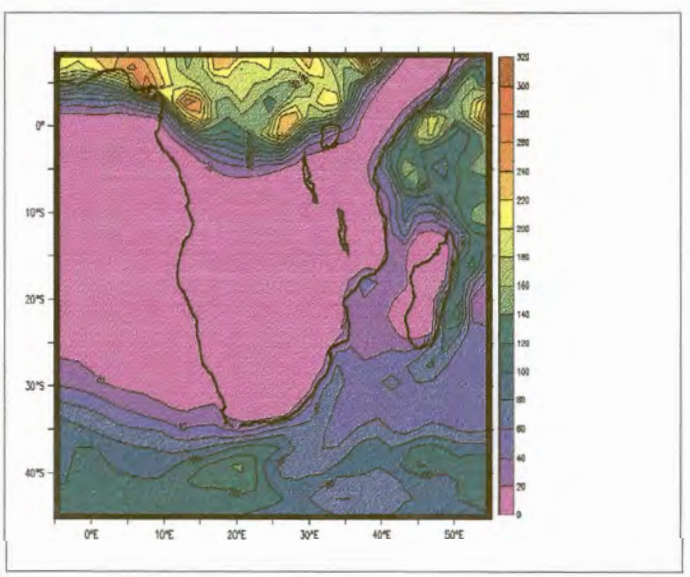


**Figure 5.6b** Observed rainfall total climate measured in mm for July as obtained from a 40-year (1958 to 1998) NCEP reanalysis climatology. The rainfall contour interval is 20 mm.

Highest rainfall figures for January occur in a north-west to south-east band located between 10°S and 20°S over Mozambique and Madagascar, with a second maximum located over the south-eastern escarpment of South Africa (figure 5.6a). Arid conditions (with monthly rainfall totals below 20 mm) have been recorded along the western coastline of South Africa, Namibia and even Angola. South of latitude 20°S, the January rainfall distribution over southern Africa is characterised by a marked west-east gradient.

During July, when the subtropical high-pressure belt establishes itself over the African subcontinent (figure 5.3b) observed rainfall totals over southern Africa decrease significantly (figure 5.6b). The ITCZ shifts to the north, inducing higher rainfalls over tropical regions north of the equator. Both Kenia and Somalia record drier conditions than experienced during January. The southern coastline of South Africa and adjacent interior is influenced by cold fronts sweeping over the area from west to east causing increased winter rainfall (figure 5.6b).

Unlike the observational (NCEP reanalysis) data, the mean January rainfall distribution as simulated by the CSIRO9 AGCM is orientated in a north-west to south-east band across the African subcontinent, with the highest rainfall figures simulated over Zambia and southern Zaire (figure 5.6c). A second distinctive rainfall maximum is located over the eastern part of Zimbabwe and north-eastern South Africa. The CSIRO9 AGCM does not capture the north-east to south-west distribution of observed maximum rainfall between 10°S and 20°S over Mozambique and Madagascar. As a result the model produces far less rainfall than observed over large parts of tropical and subtropical east Africa. The AGCM also simulates less than observed rainfall over southern Angola and northern Namibia. In contrast, the CSIRO9 AGCM simulates up to twice as much rainfall as observed over eastern Zimbabwe and north-eastern South Africa (figure 5.6c).

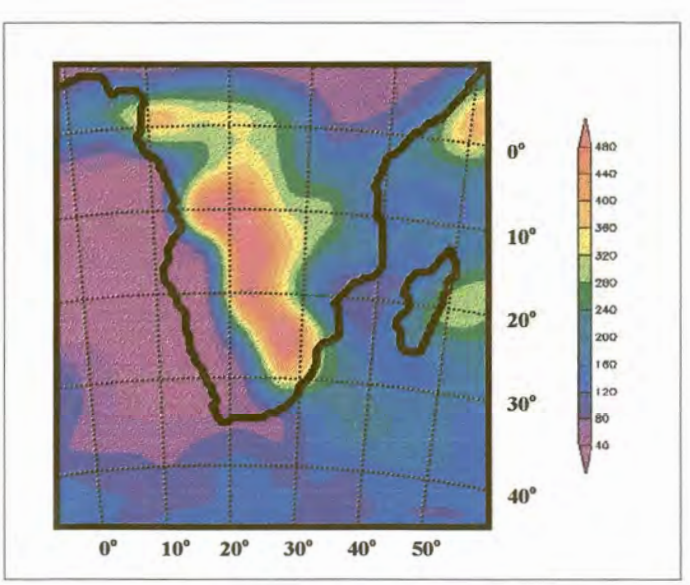


**Figure 5.6c** Rainfall total climate measured in mm for January as simulated by the CSIRO9 AGCM.

The July CSIRO9 AGCM simulation successfully captures the northward displacement of the ITCZ and subsequent drier conditions over Kenia and Somalia (figure 5.6d). The model adequately simulates the generally drier conditions that occur over the subcontinent during the austral winter. Rainfall totals increase over the south coast of South Africa, in harmony with the observed pattern (figure 5.6b).

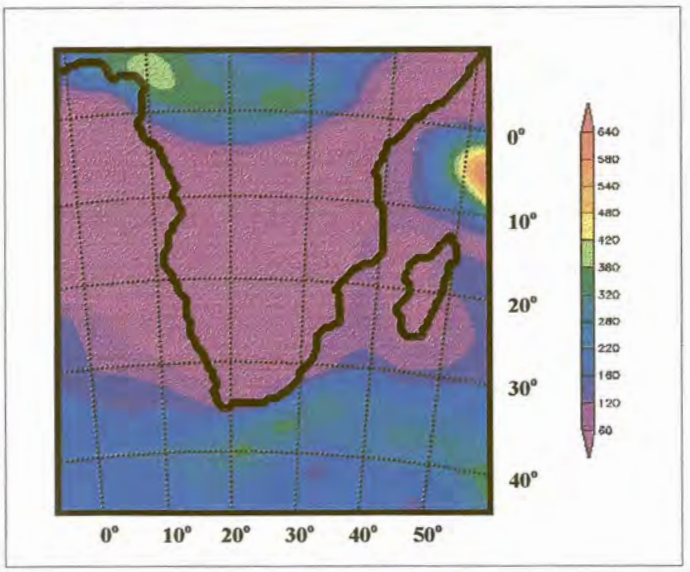


**Figure 5.6d** Rainfall total climate measured in mm for July as simulated by the CSIRO9 AGCM.

The mean January (figure 5.6e) rainfall distribution as simulated by DARLAM is orientated more from west-east than simulated by the CSIRO9 AGCM (figure 5.6c). This represents an improvement in the DARLAM simulated rainfall pattern. The difference between the two simulations is most notable over the eastern parts of South Africa and northern parts of Mozambique and Madagascar (compare figures 5.6c and 5.6e). Over both areas DARLAM simulates more rainfall than observed, compared to the less than observed rainfall simulated by the CSIRO9 AGCM. The pattern of rainfall maximums however, occurring between 10°S and 20°S over northern Mozambique and Madagascar with a second maximum located over south-eastern South Africa, is well captured in the DARLAM simulations.

In general, the DARLAM simulated rainfall pattern over tropical regions is superior to that of the CSIRO9 AGCM. In the DARLAM simulation there is some indication of the rainfall maximums observed over Gabon and Tanzania (compare figures 5.6a and 5.6e). There is no indication of the occurrence these maximums in the corresponding AGCM simulation (figure 5.6c). The DARLAM improvement in the simulated pattern of summer rainfall over the tropics (relative to the CSIRO9 AGCM) probably results from an improved representation of the southward extension of the ITCZ and low-level convergence. A comparison between the CSIRO9 AGCM simulated mean

January low-level streamlines (figure 5.4a) and the associated DARLAM simulations (figure 5.4c) reveals that DARLAM simulates more pronounced low-level convergence in tropical regions south of the equator during January.

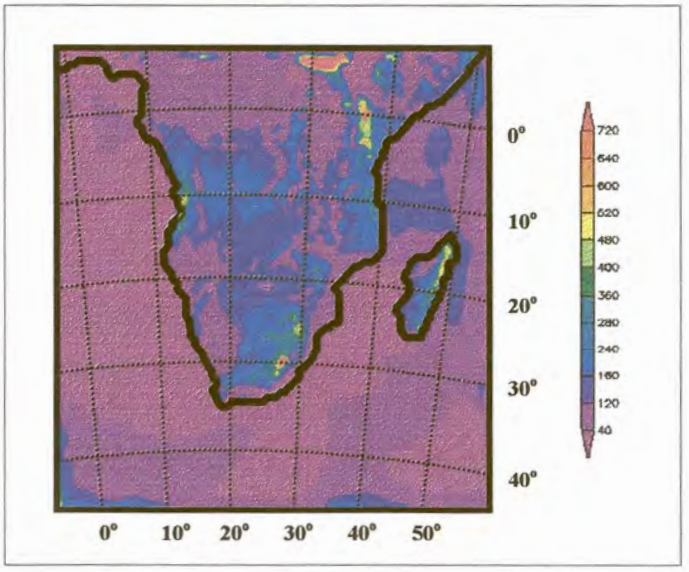


**Figure 5.6e** Rainfall total climate measured in mm for January as simulated by DARLAM.

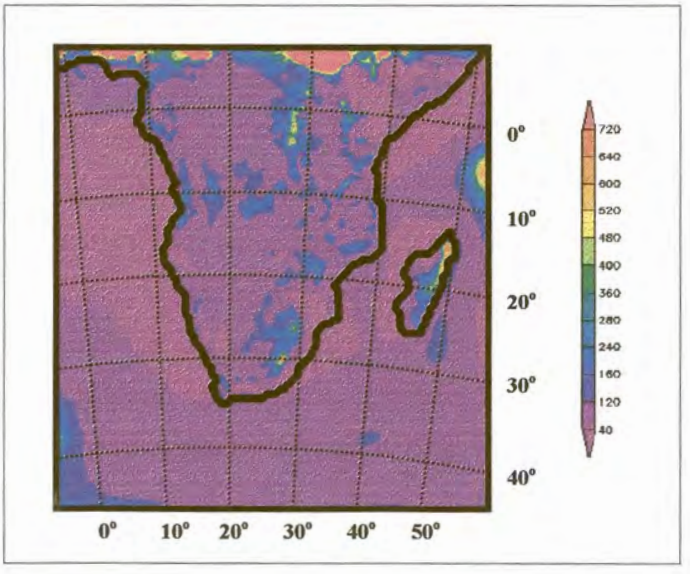


**Figure 5.6f** Rainfall total climate measured in mm for July as simulated by DARLAM.

The northward displacement of high rainfall totals in the DARLAM simulation for July (figure 5.6f) suggests that the northward displacement of the ITCZ in the AGCM simulation is adequately transferred to DARLAM through the lateral boundary forcing. Unfortunately DARLAM severely overestimates rainfall totals over the south-eastern escarpment of South Africa and the northern escarpment of Madagascar (figure 5.6f). The overestimation may be enhanced by the failure of DARLAM to capture the intensity of the subtropical high-pressure belt (and the associated subsidence) during the austral winter.

DARLAM and the CSIRO9 AGCM overestimate rainfall along the steep escarpment of south-eastern South Africa during January but the overestimation is far more severe in the DARLAM simulations. This is well illustrated in figure 5.7a, which represent differences in rainfall totals between DARLAM and the CSIRO9 AGCM for January. None the less, the DARLAM simulated pattern of a west-east distribution of rainfall over the south-eastern South Africa (figure 5.6a) is a good representation of observed fields (figure 5.6a). DARLAM simulations (figure 5.6e) incorporate far greater complexity in simulated rainfall patterns than is captured by the AGCM with its coarser resolution (figure 5.6c). Along the escarpment, close to the mountains of Lesotho and the southern Drakensberg, DARLAM rains are up to three times the observed values (figure 5.6e). During rainfall events over this area, the lower tropospheric flow up-slope (perpendicular to the topographic obstacle) and the penetrating surface moisture is advected from the east where it originates from a ridging anticyclone (Joubert et al., 1999). It has been motivated in section 5.4.1 that DARLAM produces improved simulations (relative to the CSIRO9 AGCM) of the ridging high-pressures (and the associated low-level mass convergence) along the south-eastern escarpment of South Africa during January. This may partially explain why rainfall totals in this region are higher in the DARLAM simulations (figure 5.7a).

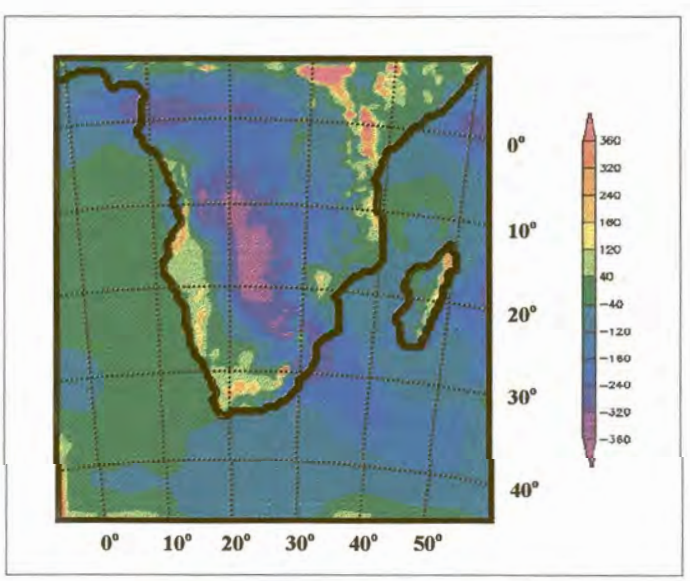


**Figure 5.7a** DARLAM minus CSIRO9 AGCM rainfall totals measured in mm for January.

The CSIRO9 AGCM also overestimates rainfall totals over the same region, although less than DARLAM. This might result from large quantities of moisture that are transported by the forcing AGCM simulations to the eastern part of South Africa. The mountain resonance effect, a phenomenon present in semi-Lagrangian model formulations, may also result in an overestimation of mean vertical velocities and increased rainfall over steep topographic gradients (see Chapter 3). Since the CFL criterion was satisfied in the present experiments, it is unlikely that the mountain resonance effect had a significant impact on the simulations. It is interesting to note however, that a vertical cross-section of topography and rainfall along approximately 30°S (figure 5.8) does illustrate a strong correlation between DARLAM simulated rainfall maximums and elevation peaks.

The improved representation of the Madagascar topography in DARLAM results in higher model rainfall totals than simulated by the CSIRO9 AGCM (figures 5.7a and 5.7b). The CSIRO9 AGCM simulates less rainfall than observed over Madagascar, especially over the higher rainfall region in the northern part of the island. DARLAM overestimate rainfall totals, particularly over the eastern mountain range. The overestimation is most severe during July, when DARLAM simulates more than seven times the observed rainfall amounts over the northern parts of the island.

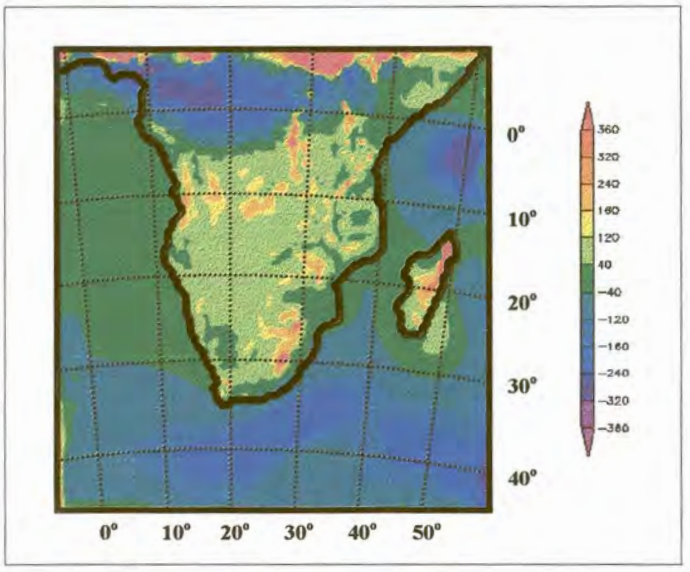


**Figure 5.7b** DARLAM minus CSIRO9 AGCM rainfall totals measured in mm for July.

Figure 5.8 depicts a vertical cross section of the DARLAM surface topography with the January rainfall climate along the 30°S latitude as simulated by DARLAM , the CSIRO9 AGCM and observed rainfall. This graph summarises the various rainfall projections over an area with relative steep topography.

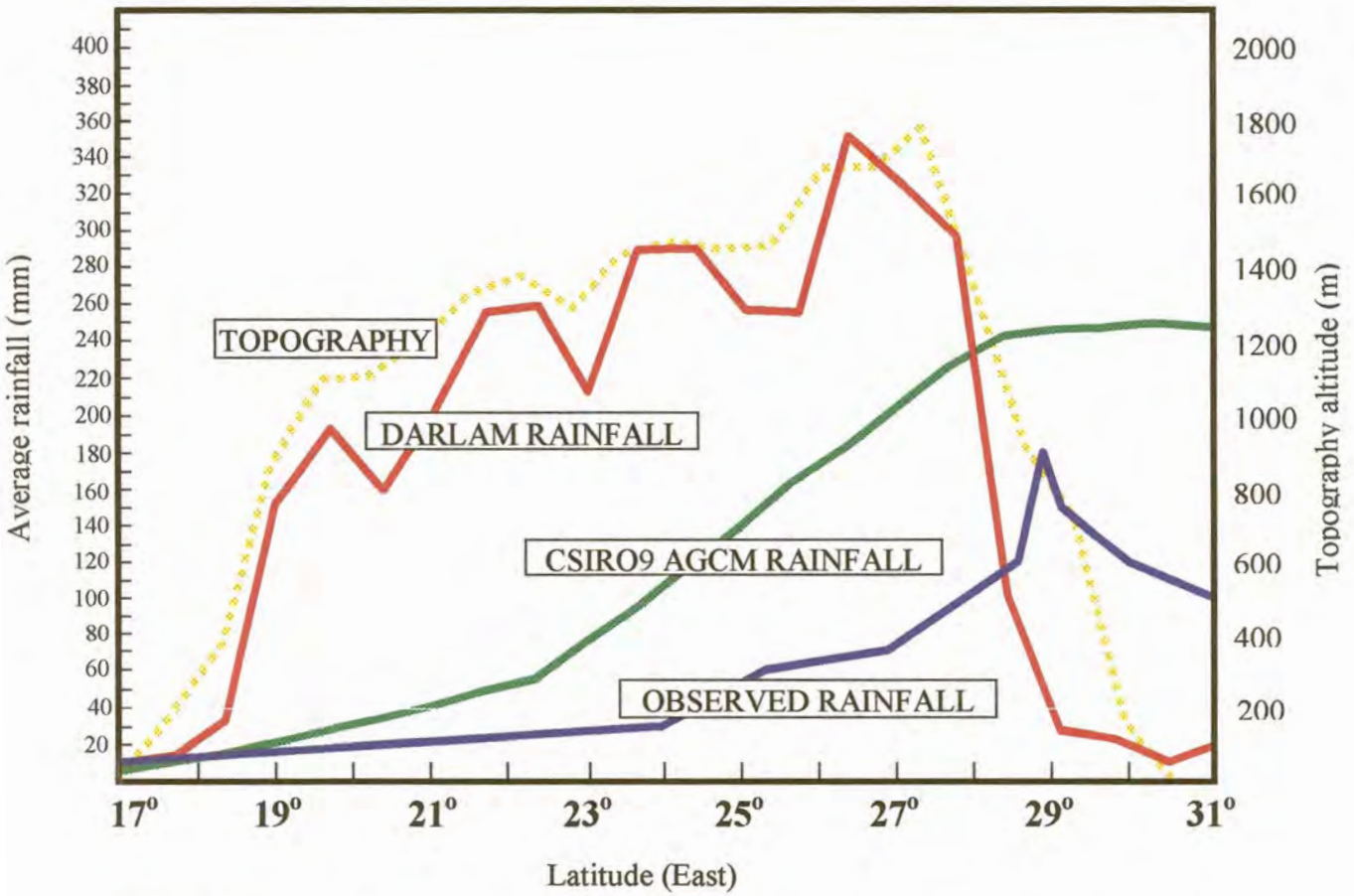


**Figure 5.8** A vertical cross section of the DARLAM surface topography measured in meters (brown dotted line) with the January (summer) rainfall climate measured in mm along the 30°S latitude as simulated by DARLAM (red line) and the CSIRO9 AGCM (green line). The associated observed rainfall graph is depicted in blue. Note the high rainfall totals along the eastern escarpment.

## 5.5 DISCUSSION

DARLAM generally provides a more accurate and detailed simulation of climate over the SADC region than the CSIRO9 AGCM. This may be attributed to the fact that topographical features, which have an influence on the climate of the region, are more clearly resolved at the 60 km resolution of the nested model than they are by the CSIRO9 AGCM. These features include the escarpment along the south-eastern part of South Africa and the Great East African Valley. The resulting climatological patterns (in particular rainfall and surface temperature) have more detail and are more complex in DARLAM simulations than in CSIRO9 AGCM simulations. The resulting DARLAM climatology exhibits several features that are also present in the forcing CSIRO9 AGCM. For example, the northward displacement of the ITCZ and the subtropical high-pressure belt during the austral winter is closely related in the AGCM and nested model simulations.

In contrast, DARLAM's January climatology over the central parts of the model domain differs from that of the AGCM and is a better representation of observations. This is particularly true of the low-pressure cells located over Namibia and Botswana. The DARLAM January rainfall distribution between 10°S and 20°S and over the south-eastern parts of South Africa provides a better representation of the observed west-east gradient of maximum rainfall than CSIRO9 AGCM. In the latter, the rainfall pattern is aligned north-east to south-west.

DARLAM underestimates the intensity of the observed winter (July) subtropical high-pressure region over the subcontinent. This contributes to a severe overestimation of July rainfall totals over the south-eastern parts of South-Africa. In this respect the DARLAM simulation is inferior to the CSIRO9 AGCM simulation that successfully captures the intensification of the subtropical high during winter.

DARLAM simulations produce more than twice the amount of rainfall observed over regions with steep topographic gradients, such as the South African eastern escarpment and Madagascar. This result has also been noted in other atmospheric models (Giorgi et al., 1994, McGregor and Walsh, 1994, Walsh and McGregor, 1995, Jenkins and Barron, 1997). The overestimation may be attributed to the fact that too much moisture is available in the model domain. Because DARLAM successfully captures events of low-level mass convergence along the eastern escarpments of South Africa and Madagascar, the excess of moisture may result in simulations with excessive rainfall. Another possible contributing factor to the overestimation of rainfall is the mountain resonance effect (Rivest and Staniforth, 1994; McGregor, 1997a) which may be present in DARLAM's semi-Lagrangian dynamical formulation. It should be noted that the solution advocated by Rivest and Staniforth (1994) to the mountain wave resonance problem is not incorporated in the DARLAM code used in the present study. The effectiveness of the proposed solution over the steep eastern escarpment of South Africa needs to be investigated in future experiments.

Despite the problems that occur when simulating observed rainfall magnitudes over regions of steep topography, DARLAM provides a more accurate simulation of observed rainfall distribution, particularly in regions where the AGCM's coarse resolution does not permit regional topographic features to be resolved. These preliminary simulations indicate that DARLAM is capable of simulating details on the regional scale with greater skill than the CSIRO9 AGCM.